Available online at www.sciencedirect.com

SciVerse ScienceDirect

Acta Materialia 61 (2013) 494–510

Acta MATERIALIA

www.elsevier.com/locate/actamat

Revealing the strain-hardening behavior of twinning-induced plasticity steels: Theory, simulations, experiments

David R. Steinmetz [a,*], Tom Jäpel [a], Burkhard Wietbrock [b], Philip Eisenlohr [a], Ivan Gutierrez-Urrutia [a], Alireza Saeed–Akbari [c], Tilmann Hickel [a], Franz Roters [a,*], Dierk Raabe [a,*]

[a] Max-Planck-Institut für Eisenforschung GmbH, Max-Planck-Str. 1, 40237 Düsseldorf, Germany
[b] Institute of Metal Forming, RWTH Aachen University, Intzestrasse 10, 52056 Aachen, Germany
[c] Institute of Ferrous Metallurgy, RWTH Aachen University, Intzestrasse 1, 52056 Aachen, Germany

Received 25 August 2012; received in revised form 12 September 2012; accepted 17 September 2012
Available online 1 November 2012

Abstract

We present a multiscale dislocation density-based constitutive model for the strain-hardening behavior in twinning-induced plasticity (TWIP) steels. The approach is a physics-based strain rate- and temperature-sensitive model which reflects microstructural investigations of twins and dislocation structures in TWIP steels. One distinct advantage of the approach is that the model parameters, some of which are derived by ab initio predictions, are physics-based and known within an order of magnitude. This allows more complex microstructural information to be included in the model without losing the ability to identify reasonable initial values and bounds for all parameters. Dislocation cells, grain size and twin volume fraction evolution are included. Particular attention is placed on the mechanism by which new deformation twins are nucleated, and a new formulation for the critical twinning stress is presented. Various temperatures were included in the parameter optimization process. Dissipative heating is also considered. The use of physically justified parameters enables the identification of a universal parameter set for the example of an Fe–22Mn–0.6C TWIP steel.

Keywords: Constitutive modeling; Strain hardening; Twinning; TWIP steels

1. Introduction

Mechanical twinning is an important deformation mechanism that interacts closely with dislocation glide to provide a complex strain-hardening behavior in low stacking fault energy (SFE) face-centered cubic (fcc) metals and alloys. There have been a number of proposed models to simulate the hardening behavior of low-SFE fcc metals that are either phenomenological or are physically-based but lack certain features, such as dislocation cells, and the ability to predict the influence of temperature and/or strain rate on deformation behavior over a wide domain of parameters. A number of physically based models describing the strain-hardening response of low-SFE fcc metals exist [1–6] which are capable of describing several deformation stages as well as twin–slip, slip–slip and twin–twin interactions.

When looking beyond these approaches, we found that new experimental investigations have revealed additional important microstructural features, such as networks of dislocation cells and the connection between the existing dislocation substructure and mechanical twinning, ignored in previous models [7–9]. Also, recent ab initio predictions have provided us with reliable and physics-based parameter values and revealed important chemical and thermal trends in the SFE, elastic properties and heat capacity of these alloys [10–13].

* Corresponding authors.
E-mail addresses: d.steinmetz@mpie.de (D.R. Steinmetz), f.roters@mpie.de (F. Roters), d.raabe@mpie.de (D. Raabe).

1359-6454/$36.00 © 2012 Acta Materialia Inc. Published by Elsevier Ltd. All rights reserved.
http://dx.doi.org/10.1016/j.actamat.2012.09.064

Our new approach not only incorporates these recent findings but also introduces a multiscale plasticity modeling concept whereby ab initio derived quantities are linked with constitutive microstructure evolution equations that are based on internal variables. The main use of such a model is that it provides insight into the mechanisms active in producing the high strength and, more importantly, the concurrent high formability of these materials. It can also deliver initial input variables for a crystal plasticity model built upon the same principles, similar to previous models, such as those developed by Ma et al. [14,15].

The cause of the high strain hardening in low-SFE fcc alloys, particularly high-Mn steels, has been widely discussed [16–25]. Two schools of thought exist. The first states that the interstitial C atoms of C–Mn dipoles interact strongly with dislocations [19]. The bond to the substitutional Mn holds the interstitial atoms in place in the lattice, producing a dynamic strain aging effect. The second idea is that mechanical twins provide barriers to dislocation motion, increasing dislocation storage and thus decreasing their mean free path [25]. Dislocation reactions at twin boundaries have been proposed by Venables [26] and Friedel [27] to support the idea that twin boundaries can be treated as grain boundaries, and these observations were supported by transmission electron microscopy (TEM) images [25,28]. Presented TEM images which help explain the high strain hardening of Hadfield steels by showing the inhomogeneous activation of slip in the matrix and the twin [4].

In this article, we propose a new constitutive model based on the idea that twins produce kinematical barriers to dislocation motion. There are several new aspects to this model: (i) twin nucleation and growth are separated, and the nucleation rate of deformation twins is directly coupled to the microstructure in terms of internal state variables and is not governed by a fitting parameter other than the size of the twin nucleus; (ii) a critical stress for twinning is introduced which corresponds to Mahajan and Chin's nucleation model [29]; (iii) the SFE is temperature sensitive and obtained from thermodynamic calculations with ab initio derived interface energies; (iv) back-stresses are decoupled from the critical stress for twin growth by including them directly in the twin nucleation mechanism; (v) the sample temperature, and therefore the SFE, critical twinning stress and dislocation annihilation rates by climb, evolve with deformation owing to dissipative sample heating; and (vi) most importantly, correct true stress–true strain and hardening behavior are predicted over a range of 293–873 K using a single and physically well justified model parameter set. In addition, the first measurements of twin volume fraction based on electron channeling contrast imaging (ECCI), which has a resolution lying between electron backscatter diffraction (EBSD) and TEM, are also presented. Coupled with stress–strain curves taken from compression tests over a wide temperature range, they are used to validate the model.

From a conceptual perspective, the novelty of the approach lies in the fact that physically based model parameters are used, that a universal constitutive model parameter set for the Fe–22Mn–0.6C TWIP steel is derived and that the approach combines ab initio derived thermodynamic quantities with a microstructure evolution model to predict twin nucleation. The latter feature enables us to conduct a new calculation of the critical twinning stress, based on the twin nucleation mechanism proposed by Mahajan and Chin [29], and to link it to microstructure evolution and to ab initio derived parameters. This enables the user to incorporate first principles information in a seamless fashion into microstructure evolution models.

To be clear, this is an isotropic model of a polycrystalline sample which does not take grain orientation into account; however, one part of the twin nucleation mechanism does provide the ability to include the average effect of the inhomogeneous activation of twin systems under a given external stress in grains of differing orientations [30,31]. It was developed in conjunction with a corresponding crystal plasticity model based on the same internal structure, which will be discussed in a later paper.

The paper is structured as follows: first, existing models for low-SFE fcc metals that twin are reviewed, followed by a review of the literature on proposed mechanisms for twin nucleation. Next, our experimental procedure is briefly described, followed by a detailed explanation of our model. Lastly, our results and a discussion thereof are presented. A conclusion finishes the paper.

2. Existing models accounting for twinning in low-SFE fcc metals (in chronological order)

Rémy presented the first model to explain the deformation behavior of low-SFE fcc metals [32]. It is an isotropic approach with phenomenological elements. He notes that several twin nucleation models are, strictly speaking, growth models, but that Mahajan and Chin's model is a true twin nucleation model [29]. New twins are considered to be thin discs whose length and volume decrease with increasing twin volume fraction. It is mentioned that the number of new twin nuclei must be linked to the dislocation density if a particular dislocation reaction is responsible for creating the twin nucleus. In the model, however, it is actually linked to the matrix strain, it being claimed that the dislocation density is related to it. Rémy takes the matrix strain as equivalent to the applied strain. In order for twins to nucleate, a favorable stress condition must exist. By linking a critical stress to a critical strain, an implicit function of strain is developed for the volume fraction of twins [33]. The work hardening due to the existence of deformation twins is attributed to the coherent twin boundaries, which impede dislocation motion and prevent dislocations from entering the twins, except in the case of complicated dislocation reactions. A Hall–Petch-like phenomenon links the contribution of twins to the flow stress. Good results were obtained for a Co–33Ni alloy at 293 K and 473 K.

Kalidindi presented a model to simulate the strain-hardening behavior of low-SFE fcc metals and incorporated it into a crystal plasticity framework [21,34,35]. The model is based on a temperature-insensitive phenomenological approach. It incorporates twinning as an additional kinematic degree of freedom for shear to the single crystal yield surface similar to slip. It accounts for interactions between the slip and twinning by allowing both to influence hardening rates on the individual slip and twin systems. The model does not include the influence of slip on twin hardening, temperature dependence, twin nucleation and twin growth. As a first attempt, the same viscoplastic power law that was used to describe the slip rate was extended to describe the evolution of deformation twin volume fraction. Since it was shown that low-SFE fcc metals show anisotropic deformation behavior following different deformation paths [18], one of the goals of the model was to predict this anisotropic strain-hardening behavior in path-change experiments. The model was successfully used to predict textures, influenced by microscale shear banding [36,37], and basic stress–strain and hardening characteristics for both simple compression and simple shear deformation paths. The hardening behavior for several low-SFE fcc metals was predicted well. Kalidindi's model provided the kinematic foundations and supplied elements used in later models, such as a phenomenological description of the change in twin volume fraction and the hardening of the twin systems with increasing strain.

Karaman et al. suggested a model for Hadfield steels which uses a power law to describe the nonlinear viscous shear rate on each slip system in each crystal [4]. A hardening formulation was introduced which includes separate parameters for the spacing of grain boundaries and twin boundaries, as well as separate parameters to describe the strength of each type of boundary as a barrier to dislocation motion [30,31]. This means that grain boundaries and twin boundaries affect dislocation storage differently. The constitutive model is incorporated into a crystal plasticity framework using a viscoplastic self-consistent approach. Twin volume fraction evolution is implemented using the predominant twin reorientation scheme [38], whereby a dynamic threshold twin volume fraction induces a self-adjusting behavior which ensures that the reoriented twin volume fraction corresponds to that of the real twin volume fraction. A yield strength of 110 MPa for slip and a critical stress of 115 MPa for twin nucleation were set by the authors as constants. The model successfully predicts no further twinning inside twinned regions, with regions both in twins and between twin lamellae deforming primarily by slip; slip between the twin lamellae, however, plays a more dominant role in accommodating the plastic deformation. Three different average grain sizes were modeled: 100 μm, 300 μm and 1.0 mm. The model correctly predicts the stress–strain response for coarse-grained (300 μm and 1.0 mm average grain size) Hadfield manganese steel, showing good agreement with experimental stress–strain curves measured at room temperature. However, the random texture in the 100 μm polycrystal materials produced predominantly slip and the simulation did not capture the upward curvature of the stress–strain curve. The twin reorientation scheme allowed for accurate predictions of hardening behavior and texture evolution in single and polycrystals.

Bouaziz and Guelton introduced a physics-based model which accounts for the interaction between twinning and dislocation motion by incorporating the characteristic spacing of twins into the dislocation storage [3]. The dislocation density and twin volume fraction are the microstructural state variables. The evolution of dislocation density is a combination of dislocation multiplication and annihilation which includes the mean free path (MFP), while the evolution of twin volume fraction is a function of the existing twin volume fraction, strain and a model parameter dependent on the SFE.

Allain et al. extended Bouaziz and Guelton's model to use the Franciosi interaction matrix to include slip–slip interactions [39,1]. The MFP of dislocations and the evolution of dislocation density are calculated in a similar manner to the Bouaziz and Guelton model, with the exception that a symmetrical slip–twin interaction matrix is used to model cross-hardening from non-coplanar slip and twin systems. They were also the first to include temperature dependence in the viscoplastic shear rate formulation in a constitutive model of low-SFE fcc metals that twin. Following Rémy, a more sophisticated description of the evolution of twin volume fraction which considers the volume of a newly formed twin is presented [32]. The critical stress for twinning has three components: back-stress due to the extension of a stacking fault, self-stress due to dislocation curvature and stress due to dislocation pile-ups. In conjunction with the applied stress, a twin nucleation rate for each twinning system is calculated. Good agreement between constitutive model simulations and experiments are seen at room temperature and 673 K regarding the stress–strain response; the dislocation MFP, which is the average distance a dislocation travels before becoming stored; and the number of grains which had one or two twin systems activated.

Cherkaoui presented a crystal plasticity model for deformation behavior of low-SFE fcc metals [40]. Twins are treated as expanding ellipsoidal inclusions using an extended energy balance from Eshelby, and slip and twinning both have individual flow rules. The purpose of the model was to exploit the competition between slip and twinning, and showed promising results when compared to experimental data from literature.

Bouaziz et al. introduced the Bauschinger effect (BE) to explain the effect of grain and twin boundaries on the hardening mechanisms in TWIP steels [41]. It built on Bouaziz's and Allain's previous models [3,39,1]. A back-stress due to the kinematical hardening produced from the BE was added to the flow stress. It included a factor for the number of dislocation loops piled-up at a boundary, whose evolution with strain was given. Only one fitted model parameter

was introduced to account for this extra stress component, namely, the maximum number of dislocation loops at a boundary. The Kocks–Estrin (KE) dislocation density evolution equation was updated to include the BE, and a new empirical equation for the evolution of twin volume fraction was presented. The grain size effect and back-stress simulations matched experiments well, and it was shown that the critical strain for onset of twinning increases with grain size, but the stress at the critical strain was always 550 MPa. Mingxin et al. used this same model to show the maximum number of dislocation loops at a boundary is a linear function of the carbon content [42].

The constitutive model introduced by Shiekhelsouk et al. [5] is built from the grain level up [5]. A polycrystal is taken as the representative volume element, and grain orientations are assigned. The constitutive model was incorporated into a self-consistent crystal plasticity framework. The single-crystal viscoplastic strain rate for slip is the sum of the product of the Schmid tensor and the slip rate on each system, while that for twinning is the sum of the product of the Schmid tensor for twinning systems, the characteristic twinning shear and the instantaneous rate of twinning. Twinning is not allowed in twinned regions, and no twin reorientation scheme was employed. Both temperature and rate dependence are incorporated into the slip rate. The plastic spin tensor is used to calculate lattice rotations based on crystallographic slip. These rotations are the primary contributor to texture evolution due to the small volume fraction of twins. The shear stress is directly linked to the total forest dislocation density. Activated twin systems that are non-coplanar to the active slip system, grain size and dislocation density are included in the calculation of the MFP by a harmonic mean. A power-law-type evolution law was used to model twin kinetics. The temperature dependence of the critical shear stress for twinning is represented by the temperature dependence of the SFE [43]. The increasing resistance to twinning is exhibited through twin–twin interactions [44], which are represented here by hardening equations first proposed by Kalidindi [21]. Slip parameters were fitted against experimental data at 673 K, where no twinning should exist. Twin parameters were fitted at 298 K. There was a good correlation between the experimental and simulated stress–strain curves for the two temperatures. In the one hardening curve shown, the hardening increases slightly after its initial precipitous decline, but fails to capture the hump characteristic of high-Mn TWIP steels. Good correlation was observed between the fraction of grains showing zero, one or two active twin systems, as well as with the dislocation mean free path due to twinning.

Kim et al. introduced a constitutive model for Al-TWIP steel which included the effect of dynamic strain aging (DSA) [45]. It uses a modified KE model of coupled mobile and forest dislocations whose evolution contributes to hardening by the constriction of their MFP by twins. The twin volume fraction evolves according to the phenomenological law first proposed by Bouaziz et al. [41]. An additive term for DSA is included in the flow stress calculation. Twinned and untwinned grains are treated separately, and the rule of mixtures is used to combine the two. The model parameters were fitted to experimental observations of dislocation density by TEM and the fraction of twinned grains by EBSD, providing good results for a single room-temperature tensile flow curve. It was concluded that the contribution of DSA to the overall flow stress is minor.

Dancette et al. presented a crystal plasticity model for texture development and hardening in TWIP steels [6]. One purpose of the paper was to compare three different scale transition schemes from the grain scale to the macroscale: a multisite model, a Taylor-type model and crystal plasticity finite element modeling (CPFEM). The hardening is governed twofold: by the restriction of the MFP of dislocations calculated by a harmonic mean, including grain size, dislocation density and the twin volume fraction (through Fullman's analysis); and by dynamic recovery through the Kocks–Mecking–Estrin model. Dancette et al. [6] use Kalidindi's framework [34] for deformation by twinning in the parent grain; no mention of twin volume fraction evolution is made, leading to the assumption that it is the same as Kalidindi's. The model matches the stress–strain and hardening behavior of unstrained and pre-strained samples in tensile tests at room temperature. Twin volume fraction data were obtained from EBSD scans, making assumptions to account for the large difficulty in indexing the nanotwin lamellae with the EBSD technique. This allowed direct comparison of active twin systems, grain average orientation and twin orientation for a large number of individual grains. Simulation of texture evolution, lattice orientation of the twins and twin volume fraction evolution for non-prestrained tensile test samples at room temperature match experimental data quite well. Considering the scale transition schemes, the multisite model was determined to be a good, computationally sparing approach (compared to CPFEM) for up to moderate strains (30%), while CPFEM was best at large deformations. At the grain level, the multisite model and CPFEM were better than the isostrain (Taylor) or isostress approaches.

Barbier et al. [2] presented a crystal plasticity model, based on Shiekhelsouk et al.'s model [5], in which a representative volume element of 3000 grains was considered. Two homogenization schemes were tested, the Taylor approximation and the translated field model. Anisotropic dislocation slip and twinning were considered using a Kocks–Mecking dislocation density evolution model coupled with a harmonic calculation of dislocation MFP which included grain size, dislocation density and twin interfaces. The evolution of the critical twinning stress was calculated according to Kalidindi's phenomenological hardening law. The evolution of the twin volume fraction accounted for the evolving critical twinning stress, but it uses a phenomenological reference twinning rate. The main purpose of this paper was to investigate and predict texture evolution over multiple strain paths (transverse direction tension, rolling

direction tension and rolling direction simple shear). The model results matched experimental results well for all three loading paths, and showed that the simple shear test rotates grains so that they are in an unfavorable orientation for the activation of multiple twinning systems. Because an active twin system non-coplanar to the primary active system inhibits further twin growth, the overall twin volume fraction was higher for simple shear than for both tension tests, where many grains were rotated into favorable orientations to activate a second twin system. The texture, however, was controlled primarily by crystallographic slip.

3. Earlier proposed twin nucleation mechanisms in fcc metals

3.1. The pole mechanism for twin nucleation

Cottrell and Bilby proposed the first mechanism to describe the nucleation and growth of mechanical twins [46]. Their theory focused on the shear produced by partial dislocations moving in the twinning plane, knowingly ignoring the often necessary localized rearrangements of neighboring atoms.

The Cottrell–Bilby mechanism considers three dislocations, b_1, b_2, and b_3, meeting at a node, where b_1 and b_2 do not lie in the slip plane of b_3. Each revolution of b_3 about the dislocation node, where b_1 and b_2 lead out of the slip plane, produces a simple shear on the slip plane if the Burgers vectors of b_1 and b_2 also lie in the slip plane. However, if they have a component normal to the slip plane whose magnitude is equal to the plane spacing, one revolution of the slip dislocation about the pole will cause a displacement from the origin of one atomic layer. The pole dislocation must be sufficiently anchored that it is immobile under the stress moving the sweeping dislocation. The climb of the dislocation around a helical surface formed due to the perpendicular component of the Burgers vector is the core idea of the pole mechanism. In the fcc lattice, if sufficient energy is available from external sources, the dissociation of a perfect dislocation whose dislocation line lies in one of the (1 1 1) planes into a Shockley partial dislocation and a Frank sessile dislocation can occur, e.g.

$$\frac{a}{2}[110]_{(1\bar{1}1)} \rightarrow \frac{a}{3}[11\bar{1}]_{\text{sessile}} + \frac{a}{6}[112]_{(11\bar{1})} \quad (1)$$

The perfect dislocation and the Frank dislocation both have Burgers vectors equal to one (1 1 1) spacing, rendering them suitable pole dislocations. Because both the Frank sessile and the Shockley partial dislocation reside in the (1 1 1) plane, the Shockley partial will meet the Frank sessile as it sweeps around the pole dislocation. Only one revolution can occur, resulting in a monolayer stacking fault. In addition to the Frank sessile acting as a barrier, another revolution of the sweeping dislocation on the (1 1 1) plane would result in an illegitimate stacking sequence where nearest neighbors are not close-packed.

To solve this problem, Venables suggested a modified pole mechanism [47]. Analogous to Cottrell and Bilby, a prismatic dislocation dissociates into a Frank sessile and a Shockley partial, creating a stacking fault. After one revolution about the pole, they recombine to form the original perfect dislocation, leaving behind a stacking fault layer. The perfect dislocation is free to glide prismatically to the neighboring close-packed plane, where the dissociation can again occur and the process can repeat itself. Repeated operation of the source on consecutive close-packed planes produces a twin. Venables [47] used experimental data of Blewitt et al. [48] in consideration of the source dislocations of such a mechanism. Glide sources – those perfect dislocations and their corresponding partial dislocations which exist in the slip plane – were shown to require either compressive, rather than tensile, stresses in order to extend the stacking fault or prohibitively high applied shear stresses and short source lengths. Those dislocation reactions which calculations indicate to be most favorable for twinning are not observed experimentally. Glide sources were thus ruled to be highly unlikely to nucleate twins. The three perfect prismatic dislocations that are not in the primary slip plane are considered as twin sources. According to experiments, one is deemed unimportant because the shear stress acting on the Shockley partial is never high. Only one of the two remaining dissociations will lead to an expansion of the intrinsic fault. Therefore, the same type of dissociation seen in Eq. (1) is important for twinning on the primary twin plane. It was reasoned that the most probable way for the prismatic $a/2[1\,1\,0]$ dislocation to acquire an extended jog on the primary twin plane is by repeated intersection with a Frank–Read source on the primary slip plane.

The Shockley partial dislocations rotating in opposite directions around the poles will meet one atomic plane apart and will not be able to pass one another. Seeger [49] suggested that passage would be possible if the twinning partial acquires enough kinetic energy. However, Venables argued that it is not necessary for the passing stress to be overcome by kinetic or applied energy if repeated activation of the twin source occurs. Unit jogs along the prismatic dislocation in the slip plane one level above the stacking fault are expected to have a lower energy than multiple jogs if the pole dislocation's nature is not entirely of a screw character. In addition, the twin source can dissociate easiest when it is on the atomic plane above the stacking fault. For this reason, unit jogs are preferably formed, and the dislocation dissociation takes place, reactivating the twin source. Another monolayer stacking fault emerges. Partials of opposite sign annihilate where the two monolayer stacking faults meet, resulting in a bilayer fault with partial dislocations at each end.

The pole mechanism can be questioned because of the very high static passing stress required for the first revolution about the pole. For the most conservative case of two partial screw dislocations passing one another separated by a single $\langle 1\,1\,1\rangle$ interatomic spacing, the passing stress for Fe–22Mn–0.6C TWIP steel is 3.6 GPa. It is possible that dislocation inertia helps in overcoming this, but to our knowledge this has not yet been clarified.

3.2. Alternative mechanisms for twin nucleation

Cohen and Weertman proposed a twin nucleation model consisting of a specific dissociation of perfect dislocations due to dislocation pile-ups at Cottrell–Lomer locks which is normally not energetically favorable [50,51]. Due to the pile-up stress, Shockley partial dislocations are forced together and the perfect dislocations are able to split into sessile Frank partial dislocations of the $a/3[1\,1\,1]$ type and glissile Shockley partial dislocations of the $a/6[11\bar{2}]$ type. This is the same reaction that Venables proposed as the basis of his modified pole mechanism, though he gave no reason as to why this particular reaction should take place [47]. This reaction should not normally occur, however, because the dislocation energy remains constant. In contrast, a dissociation into two Shockley partials lowers the overall energy of the dislocation. Cohen and Weertman justify the dissociation by claiming that the appropriate stress factor is generated at dislocation pile-ups.

The Shockley partial is formed in the conjugate slip plane and glides away from the sessile Frank partial, forming an intrinsic stacking fault. Many Cottrell–Lomer locks are created on parallel planes in a slip band which become the source of multiple stacking faults. In order for a twin to form, these stacking faults must be on directly adjacent atomic planes. Twins produced in this manner would be imperfect, exhibiting a series of matrix and twin lamellae, since not every twin plane in a large volume would have a stacking fault.

Fujita and Mori proposed a stair-rod cross-slip mechanism similar to that of Cohen and Weertman [52]. Perfect dislocations on the conjugate slip plane interact with groups of dislocation dipoles on the primary slip plane (instead of dislocation pile-ups in the case of Cohen and Weertman [50,51]), which provide strong barriers to dislocation motion. Here a stair-rod cross-slip process is initiated whereby a sessile Frank partial dislocation on a (1 1 1) plane and a glissile Shockley partial dislocation on the primary slip plane are produced according to the following type of reaction:

$$\frac{a}{2}\langle 1\bar{1}0\rangle \rightarrow \frac{a}{6}\langle 1\bar{2}\bar{1}\rangle + \frac{a}{6}\langle \bar{1}21\rangle;\ (BA \rightarrow B\gamma + \gamma A) \quad (2)$$

$$\rightarrow \frac{a}{6}\langle 1\bar{1}\bar{2}\rangle + \frac{a}{6}\langle 0\bar{1}\bar{1}\rangle + \frac{a}{6}\langle \bar{1}21\rangle;\ (\rightarrow B\alpha + \alpha\gamma + \gamma A) \quad (3)$$

$$\rightarrow \frac{a}{6}\langle 1\bar{1}\bar{2}\rangle + \frac{a}{3}\langle 1\bar{1}\bar{1}\rangle;\ (\rightarrow B\alpha + \alpha A) \quad (4)$$

The dislocation reactions according to the convention of Thompson's tetrahedron are shown in parentheses.

Miura et al. [53] proposed a twin nucleation model based on dislocation pile-up at a Lomer dislocation at the junction of the primary plane and a cross-slip plane. Two Shockley partial dislocations and a Frank sessile dislocation are created in the dislocation reaction. These subsequently create a double-layer stacking fault which serves as the twin nucleus. The model is referred to in the literature as the MTN (Miura–Takamura–Narita) model. As the temperature increases, the stress concentration created by the pile-up is relieved by cross-slip and twinning does not occur. The orientation dependence of twinning is also considered.

Karaman et al. [4] extended the MTN model by providing an experimentally supported calculation of the critical twinning stress which was dependent on orientation, solid solution hardening, and applied stress. The original model did not include the latter two effects. An effective SFE which was dependent on the applied stress and orientation was given that could vary up to 50%. Combining these calculations with single crystal experiments, correct predictions for twinning could be made in three loading directions. The orientation dependence of the SFE also allowed for an explanation of the strong tension–compression asymmetry observed in Hadfield steels.

3.3. Three-layer stacking fault

The twin nucleus used in our model was first proposed by Mahajan and Chin [29]. It is a mechanism in which two perfect dislocations split into fault pairs and react on the primary slip plane to produce three Shockley partial dislocations on adjacent planes. The partial dislocations in each stacking fault are separated by the balance of attractive forces due to the stacking fault and the repulsive forces due to the partial dislocations. The force necessary to bring the inside partial dislocations of the two stacking faults to within a distance of 10 Å, which represents an extreme case, requires a stress concentration to be achieved by a dislocation pile-up. Due to the repulsive force between the two partial dislocations, atoms in the core of one can rearrange so that it can glide on the adjacent slip plane. If a third fault pair approaches one side of this double stacking fault arrangement, the two partials constituting the boundary of the double-layer fault can combine and move to the next adjacent layer and slip away, creating a three-layer stacking fault. The Shockley partials on one side of the fault form an interface whose Burgers vectors sum to zero, making the interface immobile under the applied stress. This leaves the Shockley partials on the opposite side of the stacking fault free to move away from the interface. The twin nuclei are formed by the reaction of perfect dislocations on two coplanar slip systems in the following reaction:

$$\frac{a}{2}\langle 01\bar{1}\rangle + \frac{a}{2}\langle 10\bar{1}\rangle = 3 \times \frac{a}{6}\langle 11\bar{2}\rangle \quad (5)$$

A schematic of the twin nucleus is shown in Fig. 1. The twins would then form when these three-layer stacking faults inside a slip band on adjacent slip planes grow into one another.

Mahajan and Chin [29],Kibey et al. [54,55] and Bracke et al. [56] showed evidence of this type of twin nucleation mechanism in fcc materials, while Karaman et al. [4] and Idrissi et al. [57] claimed that the MTN model fits with their observations. There thus appears at the moment to be no

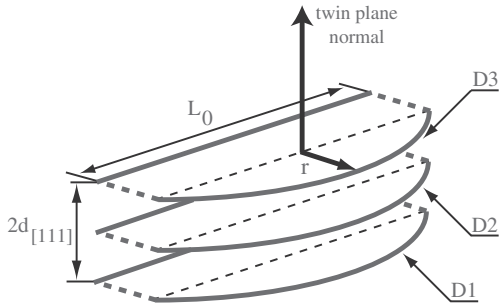

Fig. 1. The twin nucleus proposed by Mahajan and Chin and used in this model. $d_{\langle 111\rangle}$ is the interplanar spacing in the $\langle 111\rangle$ direction, L_0 is the length of the sessile partial dislocations forming the twin nucleus and r is the distance the mobile partial dislocations have bowed out. $D1$, $D2$ and $D3$ are the mobile Shockley partial dislocations which bow out to form the twin.

consensus in the literature. It may also be possible that different twin nucleation mechanisms are active under different circumstances. An overview of twinning is given in the seminal paper by Christian and Mahajan [33].

4. Experimental procedure

4.1. Materials

An overview about the effects of chemical composition, strain rate and temperature that covers the stress–strain curves used within this project is given by Wietbrock et al. [58]. That paper focuses on isothermal compression tests of three ternary high-manganese steels, with 22 and 28 mass percent manganese and 0.3 and 0.6 mass percent carbon; however, only the Fe–22Mn–0.6C material was used for the present paper.

4.2. Compression tests

The isothermal compression tests were conducted on a computer-controlled 1200 kN servo-hydraulic testing system manufactured by Servotest Ltd. The tests were conducted between room temperature (RT = 293 K) and 873 K. For all temperatures except RT, each specimen was heated up for 3 min before upsetting at the respective forming temperature inside the furnace which is integrated into the testing machine. The compression was performed nearly isothermally in a single hit to a maximum true strain of 0.7 at a constant strain rate of 0.1 s^{-1}. The friction was reduced by filling the lubrication slots with polytetrafluoroethylene. Each specimen was quenched in water immediately after compression.

4.3. Fitting procedure used for identifying a universal model parameter set

A characteristic feature of our approach is the physics-based nature of the model parameters, some of which are derived from ab initio predictions. This means that we know the order of magnitude of almost all the model parameters to be adjusted. Upper and lower bounds were hence included in the optimization function, making sure the solution is physically viable. As a fitting procedure to adjust the parameters within these bounds, an automated curve-fit process was used because many of the model parameters have strong non-linear influences on one another. In the program Matlab (The MathWorks, Inc.), the optimization function fmincon() from the Optimization Toolbox was used. This function finds the minimum of a constrained multivariate non-linear function. In addition, a custom-written particle swarm optimization function was also tested. This proved to be more robust at searching the entire parameter space, but took longer than the gradient-based method to converge upon a solution. The sum of the squared deviation between simulated and experimental data (stress–strain or hardening–strain) served as the target function, and the fitted model parameters were the variable inputs.

4.4. Microscopy

ECCI [59,60,30,61] was used for microstructural investigations. In this scanning electron microscope (SEM) technique, the grain orientations of a standard SEM sample are measured using EBSD, then individual grains are rotated into th eBragg condition, providing backscattered electron contrast near features which distort the lattice, such as dislocations [59,61]. An accelerating voltage of 10 kV was used. The resolution of ECCI is not as good as that of TEM, but the increased observable area (wide field of view) and the ease of sample preparation are major advantages [7]. ECCI was used for microstructural observations to decide which state variables should be included in the model and also for the measurement of the twin volume fraction [9].

There have been few reports on the twin volume fraction of high-Mn steels due to the morphology of the twins. Many are between 10 and 30 nm thick, making them nearly invisible to conventional EBSD. TEM is able to resolve the twins, but has a limited observable area, preventing the collection of reliable statistics. The twins often form in bundles, however, and the image quality of the EBSD patterns decreases near these twin bundles. A few authors have used the backscatter Kikuchi pattern image quality as a metric to measure the twin volume fraction [6,62,63], though quantitative information about the twin thicknesses could not be obtained.

5. Structure of the new constitutive model

Investigations of Fe–22Mn–0.6C (wt.%) using many experimental techniques, including ECCI, TEM and EBSD, have shed light on the important aspects of the microstructure of this complex class of material [7,8,62]. These are namely grain size, mechanical twins and dislocation cells. Fig. 2 presents ECCI images clearly showing

grains exhibiting dislocation cells, as well as zero, one and two active twin systems. Our approach assumes that a combination of the three-internal-variables model (3IVM) [64] with mechanical twins would describe these essential microstructural features. The important features that we have chosen to include in this model involve mobile dislocations in the dislocation cell interior, mobile dislocations inside dislocation cell walls, dislocation dipoles in the dislocation cell walls and mechanical twins. The important internal state variables are then those respective dislocation densities and the volume fraction of mechanical twins: ρ_c, ρ_w, ρ_d, f_{tw}.

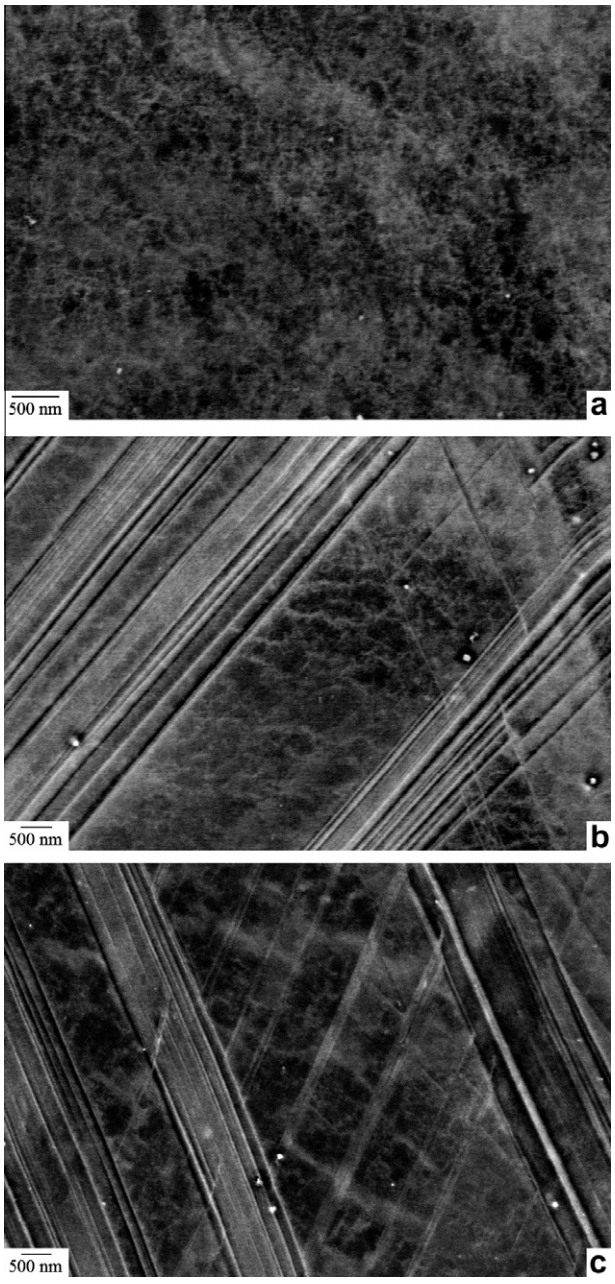

Fig. 2. ECCI images taken in an SEM of Fe–22Mn–0.6C TWIP steel at various stages of deformation: (a) dislocation cells, (b) dislocation cells with one activated twin system and (c) dislocation cells with two activated twin systems.

Table 1
Slip constants.

	Description	Value
G	Shear modulus	52.5 GPa
b	Burgers vector	2.56×10^{-10} m
$\dot{\varepsilon}$	Strain rate	0.1 s^{-1}
v	Poisson ratio	0.33
M	Taylor factor	3.06
D_0	Self-diffusion coefficient for iron	4.0×10^{-5} m^2 s^{-1}
n	Number of active slip systems	3
d	Grain size	50 μm

5.1. Evolution of dislocation densities

The evolution of the dislocation densities is given by the following equations:

$$\dot{\rho}_c = \frac{\dot{\varepsilon}M}{b}\left(\frac{1}{i_c}\sqrt{\rho_c} - \frac{2d_d}{n}\rho_c\right) \tag{6}$$

$$\dot{\rho}_w = \frac{\dot{\varepsilon}M}{b}\left(\frac{1}{i_w}\sqrt{\rho_w} - \frac{2d_d}{n}\rho_w\right) \tag{7}$$

$$\dot{\rho}_d = 2\frac{\dot{\varepsilon}M}{bn}\left\{(d_d - d_a)\left[\rho_w + \rho_c\left(\frac{f_c}{f_w}\right)\right] - d_a\rho_d\right\} - \frac{2\rho_d v_{climb}}{d_d - d_a} \tag{8}$$

where $\dot{\varepsilon} = 0.1\ s^{-1}$ is the externally imposed strain rate, $b = 2.56$ Å is the Burgers vector, $M = 3.06$ is the Taylor factor, $n = 3$ is a constant for the number of active slip systems, $f_c + f_w = 1$ are the volume fractions of the dislocation cell interiors and the dislocation cell walls, set to 0.9 and 0.1, respectively [64], i_c, i_w are parameters quantifying the average number of dislocation spacings that a dislocation moves before becoming sessile and d_a is the minimum stable dipole distance before spontaneous annihilation occurs. The symbols are also defined in Tables 1–3. The dislocation climb velocity is given by:

$$v_{climb} = \frac{D_0}{kT}\frac{G\Omega}{\pi(1-v)d_d}\exp\left(\frac{-Q_c}{kT}\right) \tag{9}$$

Here, $D_0 = 4.0 \times 10^{-5}$ m^2 s^{-1} is the self-diffusion coefficient for fcc Fe, v is the Poisson ratio, G is the shear modulus, Ω is the activation volume for climb, and Q_c is the sum of the vacancy formation and migration energies. The variables k and T are the Boltzmann constant and the absolute temperature. d_d, the maximum glide plane distance two dislocations can have to form a dipole, is calculated by:

$$d_d = \frac{Gb}{8\pi(1-v)\tau_{eff,w}} \tag{10}$$

The derivation of the evolution equations and evolution of the dislocation densities is described in detail in an earlier paper by Roters et al. [64].

Table 2
Optimized slip parameters.

	Description	Value
d_a	Minimum stable dipole separation	$1.93b$
Q_s	Activation energy for slip	4.17 eV
Q_c	Activation energy for climb	2.33 eV
Ω	Activation volume for climb	$1.53b^3$
τ_0	Solid solution contribution	72.9 MPa
α	Passing coefficient for shear	0.1
q	Top of the obstacle profile	1
p	Tail of the obstacle profile	1
$i_{c,w}$	Average dislocation spacings a dislocation travels	5.43

Table 3
Optimized twinning parameters.

	Description	Value
i_{tw}	Average twin spacings a dislocation travels	5.52
L_0	Width of twin embryo	260 nm
s	Transition profile width exponent	13.96
V	Activation volume for cross-slip	b^3

The glide resistance is calculated from the following equation [65]:

$$\hat{\tau} = \tau_0 + \alpha G b\sqrt{\rho} \tag{11}$$

Separate glide resistances are calculated for the cell interior and the cell wall due to the individual dislocation densities. The variable α is the passing coefficient for shear, G is the shear modulus, b is the magnitude of the Burgers vector, ρ is the dislocation density and τ_0 is the athermal solid solution strength component of the glide resistance.

The strain rate is expressed as:

$$\dot{\varepsilon} = \frac{\dot{\gamma}}{M} = \frac{\Lambda v_0 b \rho}{M} \exp\left(-\frac{\Delta G}{kT}\right) \tag{12}$$

where $\dot{\gamma}$ is the shear rate, Λ is the mean free path, v_0 is the Debye frequency, ρ is the mobile dislocation density and ΔG is the activation energy for slip. A modified glide resistance profile is used with the equation given by Kocks, et al. [66]. The activation energy is therefore taken as:

$$\Delta G = Q_s\left[1 - \left(\frac{\tau_{eff}}{\hat{\tau}}\right)^p\right]^q \tag{13}$$

The variables p and q are model parameters which are defined by the obstacle profile, τ_{eff} is the resolved shear stress and Q_s is the activation energy for slip. The combination of Eqs. (11)–(13) produces a strain rate given by:

$$\dot{\varepsilon} = \frac{\Lambda v_0 b \rho}{M} \exp\left(-\frac{Q_s}{kT}\left[1 - \left(\frac{\tau_{eff,x}}{\tau_0 + \alpha G b\sqrt{\rho_x}}\right)^p\right]^q\right) \tag{14}$$

where x represents c or w. The resolved shear stress is calculated individually for the cell interior ($\tau_{eff,c}$) and the cell walls ($\tau_{eff,w}$), and is combined through a mixing law to form an averaged resolved shear stress to be used later in Eq. (30) to calculate the probability of twin nucleation:

$$\sigma_{ext} = M\tau_{rss} = M(f_c\tau_{eff,c} + f_w\tau_{eff,w}) \tag{15}$$

f_c and f_w are user-defined constants which represent the volume fraction of the dislocation cell interior and dislocation cell walls, summing to one. In this case they were set to 0.9 and 0.1, respectively.

5.2. Evolution of the mean free path

In a typical Kocks–Mecking-type of constitutive model [65], in which dislocation densities are the primary state variable for describing the hardening behavior, the ratio between the increment in slipped area and the increment in (deposited) dislocation length is the decisive measure resulting in strain hardening:

$$d\rho = \frac{d\gamma}{b\Lambda} \tag{16}$$

The parameter Λ is the MFP. In reality, numerous phenomena contribute to the MFP and its change upon straining, including, but not limited to, grain size, existing forest dislocation density and, in materials that twin, the spacing of the mechanical twins.

The symbols i_c, i_w are model parameters which quantify the average number of dislocation spacings that a dislocation moves before becoming sessile. It is the analog to the reciprocal of the fitting parameter k found in similar models, but has a more tangible physical meaning here. We follow several authors [1,3,39,67] and choose to use a harmonic mean to calculate the MFP in the model presented here. There is no universal MFP in this model, but rather one in the cell interior and one in the cell wall:

$$\frac{1}{\Lambda_c} = \frac{\sqrt{\rho_c}}{i_c} + \frac{1}{d} + \frac{1}{i_{tw}t} \tag{17}$$

$$\frac{1}{\Lambda_w} = \frac{\sqrt{\rho_w}}{i_w} + \frac{1}{d} + \frac{1}{i_{tw}t} \tag{18}$$

The symbol Λ_c represents the MFP of single mobile dislocations inside dislocation cells, Λ_w is the MFP of single mobile dislocations inside dislocation cell walls, d is the grain size and t is the MFP due to twins being present. The number of twin spacings that it travels before becoming sessile in the case of twinning is i_{tw}. If dislocations travel coplanar to twins, they could travel more than one average twin spacing.

The twinning MFP evolves according to Fullman's stereological relationship [68]:

$$\frac{1}{t} = \frac{1}{2e}\frac{f_{tw}}{(1 - f_{tw})} \tag{19}$$

where f_{tw} is the twin volume fraction and e is the average twin width, or the average width of a twin bundle if they exist. A discussion of the evolution of f_{tw} follows and is presented in final form in Eq. (33).

5.3. Physical description of twin nucleation

As explained above, the twin embryo proposed by Mahajan and Chin [29] is used in our model to describe

deformation twin nucleation. A schematic of the twin embryo can be seen in Fig. 1. Three stacking faults are on adjacent parallel (1 1 1) planes. The straight back lines represent sessile Shockley partial dislocations, while the bowed out front lines represent mobile Shockley partial dislocations. The critical event for the growth of the nucleus into a twin is the bow out of the three partial dislocations between the pinning points separated by L_0. Twin growth is determined by the overall energy of the system. This has three contributions:

$$Q_{\text{work}} = -3b_s\tau_{\text{rss}}A(r, L_0) \tag{20}$$

$$Q_{\text{sf}} = \gamma_{\text{sf}}A(r, L_0) \tag{21}$$

$$Q_{\text{line}} = \frac{9}{2}Gb_sB(r, L_0) \tag{22}$$

where Q_{work} is the energy supplied by the applied shear stress τ_{rss}, Q_{sf} is the energy required to extend the stacking fault and Q_{line} is the energy required to extend the dislocation line. The symbol γ_{sf} represents the SFE, b_s is the Burgers vector of the Shockley partial, $A(r, L_0)$ is the area function and $B(r, L_0)$ is the dislocation line length.

The total energy of the system is then:

$$Q_{\text{total}} = Q_{\text{work}} + Q_{\text{sf}} + Q_{\text{line}} \tag{23}$$

For high applied stresses, the energy is constantly decreasing, but for a particular stress level a saddle point is found at $2r = L_0$, as shown in Fig. 3. The saddle point is very sharp in stress, creating a steep increase in the activation barrier for small decreases of the stress, resulting in an essentially athermal barrier stress. At this point, the mobile partial dislocations will have formed a semicircle between the two pinning points. The stress at this configuration is defined as the critical twinning stress for twin formation and is given by:

$$\tau_c = \frac{\gamma_{\text{sf}}}{3b_s} + \frac{3Gb_s}{L_0} \tag{24}$$

The SFE plays a large role in defining the critical twinning stress. Due to its strong temperature dependence, SFEs calculated thermodynamically by the method of Saeed-Akbari et al. [69] and corrected by ab initio calculations were used. More specifically, the SFEs were calculated by the sum of the molar surface density along the {1 1 1} planes and the γ/ε interfacial energy. The interfacial energy was obtained by ab initio calculations, leading to a more correct estimation of the SFEs. With this approach, the temperature-dependent SFE was updated for each deformation increment to correspond to the actual predicted sample temperature, which increased due to dissipative heating. While a suitable model has been selected to describe the twin nucleus that provides credible values of the necessary applied stress to initiate twinning, no purely physical model exists that can explain the frequency with which this event occurs, and hence the increase in twin population as a function of strain. Rémy [32] and Allain et al. [1] suggest it should be tied to dislocation density, and do so by stating that mobile dislocation activity is necessary for strain and

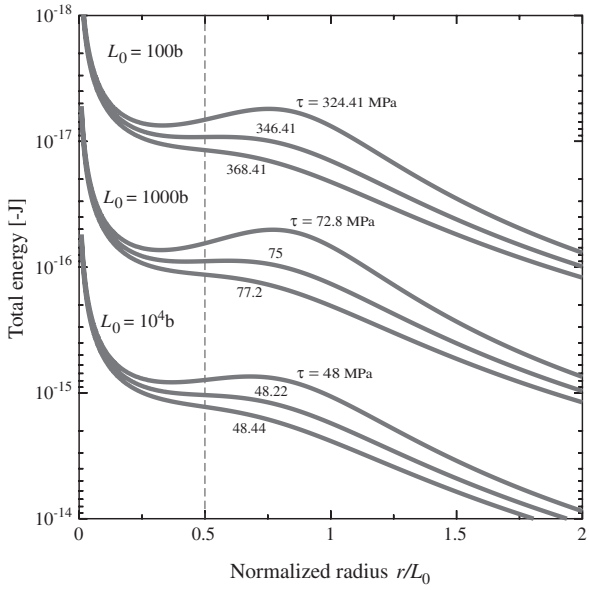

Fig. 3. Total energy (Q_{total}) of the twin nucleus. The numbers above each of the curves represent the applied shear stress. L_0 is the length of the sessile partial dislocations forming the twin nucleus and r is the distance the mobile partial dislocations have bowed out. An r/L_0 ratio of 0.5 is the critical ratio needed to be overcome in order for the twin to fully form. Less applied shear stress is required to form a twin as the size of the twin nucleus grows.

that the nucleation rate is an empirical function of strain. Allain et al. [39] link it directly to dislocation density, but an empirical constant of unknown value is included as a prefactor.

Here, we calculate the total number of potential twin nuclei based on the dislocation reaction which creates the nucleus. The number of active slip systems is a user-set parameter in the model. If the number of active systems is set to three, the probability that all three randomly chosen slip systems will all be non-coplanar is 54/110. Hence, the probability for having two active slip systems which are coplanar, fulfilling a necessary criterion for the formation of the twin nucleus, is $1 - 54/110 = 56/110$. Dislocations can only form the twin nucleus in the given model when their interaction is repulsive, i.e. 50% of the time, so an extra factor of 1/2 is included. The product of the statistical chance of forming a twin nucleus, the change in dislocation density due to dislocation multiplication accommodating the externally imposed strain rate and the reciprocal of the length of partial dislocations in one twin nucleus, $2/(3L_0)$, gives the number density of potential twin nuclei per unit time:

$$\dot{\theta} = \frac{56}{110}\frac{\dot{\varepsilon}M}{2}\frac{2}{3L_0}\rho = \frac{28}{165}\frac{\dot{\varepsilon}M}{L_0}[\rho_c f_c + (\rho_w + \rho_d)f_w] \tag{25}$$

The storage, or lifespan, of the twin nuclei is not taken into account because it is assumed that additional dislocation motion will destroy the nuclei created in the previous time step if they do not initially grow into twins.

In Mahajan and Chin's nucleation model, one bounding partial dislocation from each of two extended stacking faults on the same slip plane must come within a critical distance of one another, set as $x_c = 10$ Å for the extreme case. The equilibrium separation of Shockley partials in fcc metals is calculated by [70]:

$$x_0 = \frac{Gb}{\gamma_{sf}} \frac{b}{24\pi} \frac{2+\nu}{1-\nu} \tag{26}$$

The repulsive force between the two partial dislocations is given by [29]:

$$F_r = \frac{Gb^2}{2\pi(x_0 + x_c)} + \frac{Gb^2 \cos(\pi/3)}{2\pi x_0} \tag{27}$$

Therefore, the stress needed to bring the two partials to within the critical distance to form the twin nucleus, x_c, without help from an external applied shear stress is:

$$\tau_r = F_r/b \tag{28}$$

In order for this stress to develop, a dislocation pile-up must occur to create a stress concentration. As the dislocations pile up, the partials could be forced to recombine into the full dislocation. If the dislocation is of a screw character, it could then cross-slip to another plane and alleviate some of the stress concentration caused by the dislocation pile-up. The probability that a cross-slip event will not occur, which would instead allow a sufficient number of dislocations to pile up and form the stress concentration necessary to form the twin nucleus, is given by:

$$p_{ncs} = 1 - \exp\left[-\frac{V}{kT}(\tau_r - \tau_{rss})\right] \tag{29}$$

where V is the cross-slip activation volume.

The probability that the triple layer stacking fault bows out to form a twin is:

$$p_{tw} = \exp\left[-\left(\frac{\tau_c}{\tau_{rss}}\right)^s\right] \tag{30}$$

where p_{tw} is the probability that the nucleation event occurs, τ_{rss} is the resolved shear stress, τ_c is shown in Eq. (24) and s is a fitted model parameter determining the sharpness of the transition from the non-twinning to twinning stress domain. It can be used to represent the effect that texture has on determining which grains twin.

The total twin nucleation rate is calculated by multiplying the total number density of potential twin nuclei per unit time by the probability that a sufficient stress concentration for the formation of the nucleus exists by the probability that one of those nuclei grows into a twin:

$$\dot{N} = \dot{\theta} p_{ncs} p_{tw} \tag{31}$$

As energy is always gained during twin growth, it is assumed that twins grow instantaneously until they encounter an obstacle, such as a grain boundary or a twin on a non-coplanar twin system. A new twin is considered to be disc-shaped, where the radial dimension is based on the twinning MFP. The twin volume is given by:

$$V_{tw} = \frac{\pi}{4} e t^2 \tag{32}$$

where t is the average twin spacing from Eq. (19) and e is the average twin width. It is a constant provided from experimental observations and is set to 30 nm. The twin volume fraction evolution is calculated by the product of the nucleation rate and the volume that a new twin occupies, and can occur only in the untwinned volume:

$$\dot{f}_{tw} = (1 - f_{tw}) \dot{N} V_{tw} \tag{33}$$

5.4. Temperature evolution

Until now, constitutive models of fcc metals have not considered temperature evolution, i.e. dissipative heating, during deformation. Experiments conducted by Chen et al. [71] suggest that the temperature of an Fe–18Mn–0.6C TWIP steel can rise by more than 110 K from the starting temperature when carrying out a test beginning at room temperature. In contrast to this observation, Xiong et al. [72] reported a maximum temperature increase of 55 K for a TWIP steel deformed at a high rate of 2400 s^{-1}.

This discrepancy in the experimentally observed dissipative temperature changes is not surprising, owing to the difficulty in controlling the boundary conditions during such infrared measurements. Typical error sources in such experiments are the reflection, surface and calibration conditions. Also, differences in the experimental set-up (e.g. sample dimensions and size; strain rate) as well as the heat capacity, localization behavior and heat conduction conditions through the grips can explain deviations among the experimental results [73].

We take this discrepancy in the reported experimental heating values as a motivation for including plastic dissipation in our current model. The goal is twofold: first, we aim at predicting dissipative heating in order to evaluate corresponding experiments. Secondly, because of the temperature dependence of the SFE, cross-slip and dislocation climb rates, this effect can no longer be ignored when predicting the mechanical behavior of such materials.

The change in temperature comes from work put into the sample minus the heat that is conducted away through the die:

$$\frac{dT}{dt} = \frac{\sigma_{ext}\dot{\varepsilon}}{\varrho_{Fe} C_p} f_D - \frac{2\alpha}{\varrho_{Fe} C_p h}(T - T_0) \tag{34}$$

f_D is the dissipation coefficient, ϱ_{Fe} is the density of iron, C_p is the ab initio-calculated temperature-dependent heat capacity for iron, α is the heat transfer coefficient, h is the height of the specimen (assuming a constant heat flux), T is the temperature and T_0 is the temperature of the die, which is considered to be a constant and is equal to the starting temperature of the test. Heat dissipation by air is not considered because the transfer of heat through air is much smaller than that through the die.

6. Results

In Fig. 3, the total twin nucleus energy Q_{total} is plotted against the normalized radius r/L_0, where r is the distance representing how much the mobile Shockley partial dislocation has bowed out and L_0 represents the source length of the twin embryo (Fig. 1). The small numbers along each curve represent different values of applied shear stress. Each group of lines represents a different source length one order of magnitude apart. The size of the original nucleus is determined by L_0.

After optimization, it was possible to fit the experimental data over a wide range of temperatures with a single parameter set. Table 1 presents the constants used in the model, Table 2 the optimized slip parameters and Table 3 the optimized twin parameters.

Fig. 4 shows the flow curves for seven temperatures; Fig. 5 shows the hardening curves corresponding to the stress–strain curves in Fig. 4.

The flow curves fit to the experimental data well for all temperatures. Upon inspection of the hardening curves, it is seen that the trends for each temperature are followed, and that reasonable agreement between simulation and experiment exists. Due to the significantly more difficult issue of correctly predicting hardening behavior, these fits are considered to be quite good and represent a step forward in the constitutive modeling of fcc materials with low SFE over a broad temperature range.

Because twin interfaces play such a large role in the hardening of TWIP steels, it was necessary to determine their volume fraction as accurately as possible. Quantifying deformation twins in high-Mn TWIP steels has been tried using several different methods, including EBSD [63,6] and ESBD in combination with X-ray diffraction (XRD) [62]. The twins themselves are often between 10 and 30 nm thick, making individual twins nearly invisible to EBSD. They can be observed by TEM, but the viewable area is not as large as for other techniques and does not lead to good statistics. The challenge in XRD is to determine what exactly is a twin. It must be used in conjunction with EBSD to distinguish twins from grains in the same texture fiber. We decided to use ECCI [7,8,61,59,60], as outlined in Section 4.4.

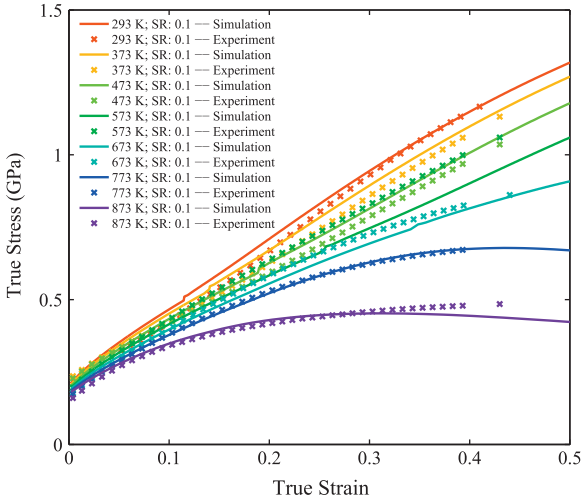

Fig. 4. True stress–true strain compression curves for Fe–22Mn–0.6C TWIP steel at seven different temperatures. One coherent parameter set was used for the whole temperature range. SR in the legend stands for "strain rate".

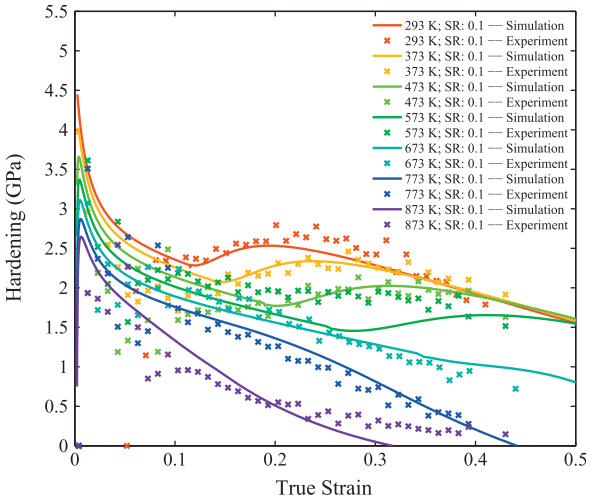

Fig. 5. Hardening curves corresponding to the true stress–true strain curves in Fig. 4 for Fe–22Mn–0.6C TWIP steel at seven different temperatures. One coherent parameter set was used for the whole temperature range.

Even if the observable area is significantly larger, it is still not an easy task to quantify the twin volume fraction: grains are heterogeneous, twins can start near the boundaries but stop in the middle of the grain, and the morphology looks quite different at high resolution and at the grain scale. The twins often form into twin bundles, which are visible at lower magnifications. High-magnification ECCI images were used to determine the average twin thickness, while ECCI images of entire grains were used to observe twin bundles and determine the twin volume fraction. The distances between twin bundles play a larger role in restricting the mean free path of dislocations than do the very small distances between individual twins in a bundle. Fifteen grains were investigated from each sample, five from each of three orientation groups: ⟨111⟩, ⟨101⟩ and ⟨001⟩. The twins were marked by hand with custom software in both the grain-level and high-resolution images. Grain boundaries were marked the same way, and the ratio of the twin bundle area to the grain area represents the twin volume fraction for each grain investigated. A numerical average of all grains represents the total twin volume fraction for the sample.

The twin volume fraction determined by ECCI is presented in Fig. 6, together with the twin volume fraction predicted by the simulation for three flow curves. The higher strain rate (10 s^{-1} as opposed to 0.1 s^{-1}) exhibits a marginally higher twin volume fraction in both the simulation and

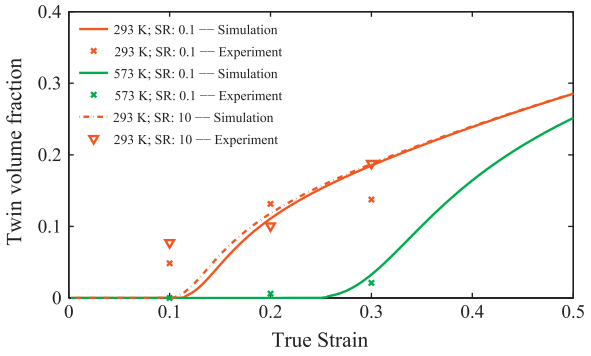

Fig. 6. Twin volume fraction obtained from the model and compared to experiments conducted by SEM-based ECCI.

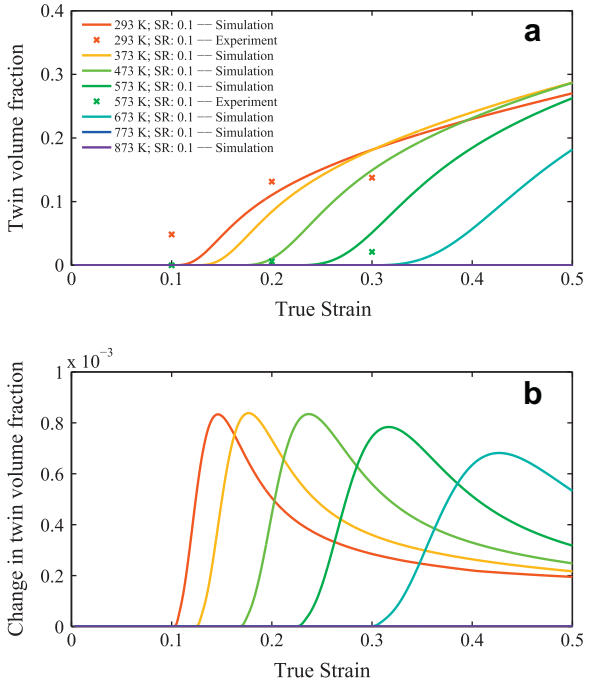

Fig. 7. Twin volume fraction (a) and the change in twin volume fraction (b) for seven temperatures. SR is the strain rate.

the experiments, but the difference was not significant. Temperature had the greatest effect on the twin volume fraction, with low levels of twinning observed at 573 K and levels between 5% and 20% at RT. A comparison of the predicted twin volume fraction for seven temperatures as well as the experimentally determined twin volume fraction for 293 K and 573 K is shown in Fig. 7a; the change in twin volume fraction is show in Fig. 7b.

The resolved shear stress is shown compared to the critical stress for twinning in Fig. 8. Both sets of lines are simulated. It is clear that, with increasing temperature and SFE, the critical stress for twinning increases during deformation. The increases in temperature, SFE and critical twinning stress are directly compared in Fig. 9.

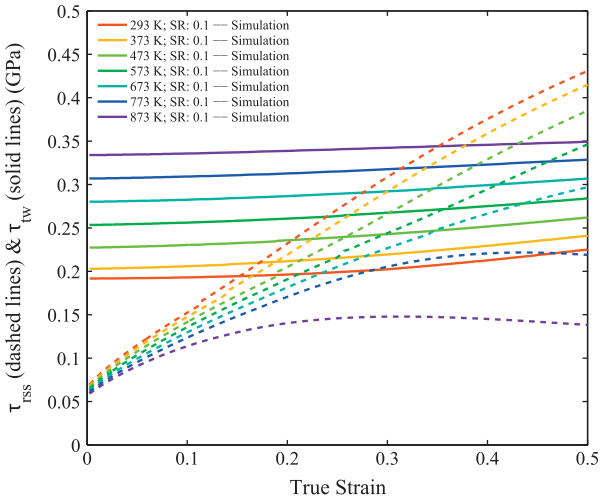

Fig. 8. Effective shear stress (dashed lines) and critical twinning stress (solid lines).

7. Discussion

The goal of this work was to develop a better understanding of the excellent strain-hardening behavior of high Mn-steels with medium to low SFE on the basis of the interaction of deformation twins and dislocations. More specifically, we are interested in the transition from conventional dislocation–dislocation-dominated hardening at low strains to the additional strain-hardening reserve due to dislocation–twin interaction observed at higher strains of TWIP steels. For this purpose, we developed here a physics-based model to ensure the use of realistic internal variables (dislocations, twins), their individual evolution equations, including twin nucleation, and their respective interactions. A further important aspect in our approach is the use of parameter ranges with physically justified upper and lower bounds.

Within this framework, we aim to reproduce and, hence, explain the origin of the secondary hardening increase of TWIP steels by using a single coherent input parameter set to appropriately predict its temperature and strain-rate dependence. The model can predict stress–strain and hardening behavior accurately. Because the hardening curve is a derivative, it is much more sensitive to mechanism changes than the flow curve. Additionally, good predictability of hardening behavior enables the delivery of information about the onset of necking using the Considère criterion. The strain-hardening rate is shown in Fig. 10, and it captures the sharp increase in hardening activity typical for this steel which has been shown in literature. Shiekhelsouk et al. [5] were not able to capture the decreasing behavior of the strain-hardening rate after the second increase, but Dancette [6] was able to do that for a simulation at room temperature. Here we were able to reproduce this trend for all temperatures. Each set of experimental data can be fitted almost perfectly with its own set of input parameters. In large-scale isothermal forming simulations, this

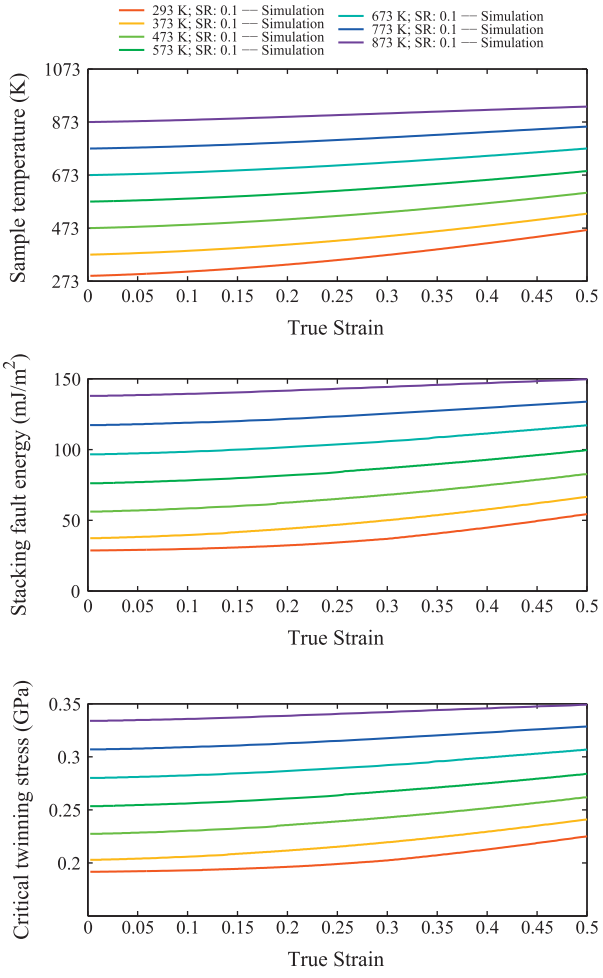

Fig. 9. Evolution of temperature, SFE and critical twinning stress at a strain rate of 0.1 s^{-1}.

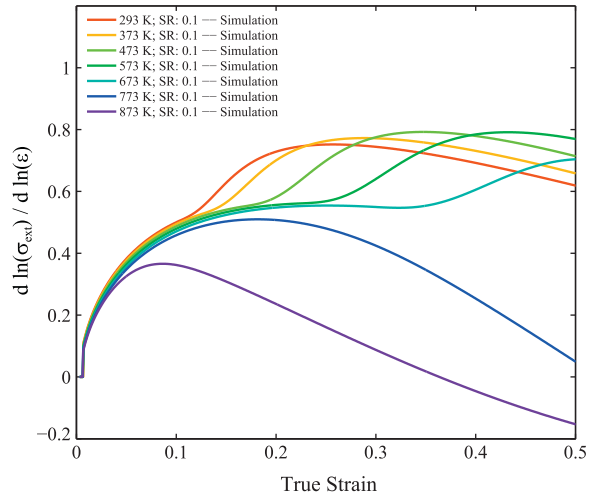

Fig. 10. Predicted strain-hardening rate. σ_{ext} refers to Eq. (15).

will produce accurate results. In simulations where the temperature and/or rate changes, a single coherent parameter set which describes material behavior over a wide range of temperatures is necessary. This is also be important in large-scale engineering and micromechanical finite element modeling [74–76] simulations in which local temperature deviations observed by infrared thermography are considered [73]. They can be in excess of 100 K as shear bands propagate through the material.

It is seen that both a critical amount of dislocation activity and a critical stress must be reached in order for twins to form. Fig. 7 shows that, once twinning is initiated, a sharp burst of twinning activity occurs, elevating the twin volume fraction quickly, after which a decrease in twinning activity occurs and a decaying twin production rate follows. Temperature clearly delays the onset of twinning by simultaneously decreasing the flow stress, increasing the rate of dislocation annihilation through climb and increasing the SFE, which in turn increases the critical stress needed to initiate deformation twinning. Temperature also spreads the burst of twinning over a larger strain range. The resolved shear stress is compared to the critical twinning stress in Fig. 8. At RT, the critical stress is breached by the resolved shear stress quite early in the flow curve, while at elevated temperatures the resolved shear stress never reaches the critical twinning stress.

The twin volume fraction predicted by the model fits well to that measured by experiment (Fig. 7). It is difficult to take measurements at strains higher than 0.3 because of the high level of deformation, so the large misorientation within a single grain prevents easy interpretation of the ECCI images. EBSD has a similar disadvantage at high deformations in that the indexing rate drops precipitously. While both experiments and the model show little twinning activity at 573 K up to 0.3 true strain, the model predicts a large increase after this. It also predicts twinning at 673 K at higher strains, which has been a temperature at which twinning was assumed to not occur. Despite these two inconsistencies, the stress-strain and hardening curves match the experimental ones very well over the whole temperature range.

From the new constitutive model, and particularly from the twin nucleation part of the model, we learn that the proper design of an SFE determines the activation stress for twin nucleation. Properly designing the SFE of the austenite as a "resistance parameter" acting against deformation twinning is essential here because, in conventional steel concepts containing unstable austenite, the resulting twinning (or martensite formation mechanisms) and the associated strain-hardening response via TWIP/TRIP often occurs at low strains, where additional hardening is usually not desired. In contrast to that, our model reveals that the design strategy in the current case should be to optimize austenite stability/SFE in such a way that twinning is activated at higher strains, where the dislocation–dislocation hardening gradually becomes exhausted. The calculated SFE can be seen in the center of Fig. 9. It increases with increasing strain due to the increase in temperature seen at the top of Fig. 9. This design principle has also been pointed out before for the case of austenitic stainless and duplex steels, where the austenite metastability must be adjusted by composition

with the aim of avoiding premature strain-induced martensite formation at too low strains [77,78].

It should be noted in that context that the dissipative heating predicted for a tensile test that starts at RT amounts to about 200 K. This value exceeds the experimental observations of Xiong et al. [72], who reported a value of 55 K for such steels, and Chen et al. [71], who reported a value of 110 K. As discussed above, we attribute this deviation between the theoretical prediction and the experiments to the difficulty in controlling the boundary conditions when taking the infrared measurements [73]. We assume that the increase in temperature during deformation predicted here is realistic since the simulation does not include any complex model assumptions or fitting parameters. This means that the deformation work is translated into dissipative heat minus the loss expressed by the relation between heat conduction and heat capacity times density (see Section 5.4).

Fe–22Mn–0.6C is both a substitutional solid solution of Fe and Mn and an interstitial solid solution of Fe and C. The effect of temperature on solid solution hardening is not explicitly considered in the model formulation, but enters through fitted values of the activation energy of the cutting process in slip and the activation energy for climb (Table 2). Including a tailored solution-hardening component would aid in extending the model to cover other compositions or material systems.

It has been suggested that the source length, L_0, should be related to the forest dislocation density [79]. Likewise, it could be related to the MFP. In this case, it was chosen to be a constant which does not change with the evolution of the microstructure. Thornton and Mitchell [80] state that, for the Suzuki model [81], L_0 should be between 250 and 500 multiples of the Burgers vector, and for Venables's model [47] it should be between 100 and 250 multiples of the Burgers vector. These are reasonable values, and the bounds of L_0 were set to be 50–1500 multiples of the Burgers vector, with the optimized value at 261 nm, or 1020b, slightly more than twice the upper limit of that predicted by Suzuki's model.

The slip strength model parameters p and q describe the slip obstacle profile. by Kocks et al. [66], their bounds should be $0 < p \leqslant 1$ and $1 \leqslant q \leqslant 2$. As was noted: "The possible range of values for p and q is limited by the requirement that the activation area increases continuously as σ decreases". The optimized slip parameters are both equal to 1 (see Table 2), indicating an average box obstacle profile. This may be due to the complex interaction of the differing strengths of forest dislocations, dislocation cell walls, twin boundaries and grain boundaries as obstacles to slip; solution hardening from the substitutional Mn atoms and interstitial C atoms; and the use of singular p and q values to describe the slip behavior in both the dislocation cell walls and the cell interior.

The fitted model parameter s controls the abruptness of the transition from the non-twinning regime to the twinning regime as a function of stress. A small value of s represents a wide transition and indicates a variation in the effect the resolved shear stress has on the nucleation and growth of new twins as it nears the critical twinning stress. Because this model does not consider individual grains and a single Taylor factor is used instead of a distribution of maximum Schmid factors to convert the external stress into a resolved shear stress, s may be used to create a profile which is consistent with the fraction of grains which have reached the critical twinning stress on a twinning system at differing orientations. This variable could provide a method to tailor the nucleation rate of twins near the transition point if the texture of an experimental sample is known. The optimized value was 13.6, indicating a sharp transition into the twinning regime.

A weight, i_{tw}, is included in the calculation of the MFP. Physically it represents the average of the number of twin spacings that a dislocation travels before being stored. It acts in conjunction with its corresponding dislocation contributions, i_c and i_w, to determine how much of a contribution twinning makes to the MFP. Therefore, it is called the twin contribution factor. The optimized value was 5.52, which is very close to that for i_c and i_w at 5.43. A larger number implies a weaker influence of the twins on the MFP, implying that twins are weaker obstacles to dislocation motion than grain boundaries, which is an idea supported in the literature [4] and by the fact that the grain boundary contribution factor is 1.

The meaningful bounds of the twin parameters have already been discussed above. Now the bounds of the slip parameters will be inspected. In Eqs. (6)–(8), d_a is the maximum slip plane separation that two dislocations of opposite sign must achieve in order to spontaneously annihilate. Its upper bound is 20 times the Burgers vector. Three more parameters in Eq. (9) are D_0, Q_c and Ω. Q_c is the activation energy of climb. This should be near the activation energy for self-diffusion, which for γ-Fe is 2.8 eV [70]. The bounds were thus set to 2.8 ± 0.5 eV. The optimized value turned out to be slightly less than for γ-Fe at 2.33 eV. Ω is the activation volume for climb, which is $1.5b^3$. In Eq. (11), α is the passing coefficient for shear, which considers the arrangement of dislocations. This has been shown to be a value on the order of unity. The bounds on solution hardening, τ_0 in Eq. (11), as a fitting parameter were 0–150 MPa. While 150 MPa may seem high, it is well known that C interstitials have a very strong hardening effect in Fe. In addition, there is a high content of substitutional Mn, the impact of which can produce further hardening not only on the Fe matrix, but also in forming couples with the interstitial C [19,82,83]. Lastly, $i_{c,w}$ represents the average number of dislocation spacings that dislocations travel before becoming sessile. This value is considered to be between 1 and 100.

8. Conclusions

A new physics-based constitutive model for low-SFE fcc metals that exhibit deformation twinning has been

developed based on a combination and extension of the 3IVM of Roters et al. [64] and the twin nucleation model of Mahajan and Chin [29]. Dislocation cells, grain size and twin volume fraction evolution are included.

Very good agreement with experimental compression data (Fe–22Mn–0.6C TWIP steel) was found between 293 and 873 K using a single set of physically motivated parameters. The model reveals that the intermediate strain-hardening regime that is responsible for the high formability of TWIP steels is due to the dynamic increase of the twin-related interface density and its interaction with the dislocations. In addition, due to the good prediction of hardening behavior over a temperature range spanning almost 600 K, the door is now open to the inclusion of adiabatic heating effects caused by shear banding, the implementation of temperature-sensitive forming simulations and the improvement of failure simulations.

The twin nucleation model introduced follows twinning at the mechanistic level and considers both the dislocation activity necessary to create twin nuclei and the stress state responsible for the expansion of the nuclei into twins. The nucleation rate of twins is linked directly to the dislocation density, the size of the twin nucleus and the SFE through the critical twin stress and the probability of formation of the twin nucleus.

The simulated temperature of the sample evolves during deformation owing to dissipation, a phenomenon that has been ignored in models until now, but is vital to include. The predicted changes in sample temperature during RT compression or tensile testing can exceed 100 K in the case studied here.

The SFE of an alloy, which is the key parameter for twinning, can nowadays be calculated ab initio by density functional theory. In combination with the presented model, it is therefore possible to tailor the SFE (i.e. the alloy composition) to achieve desired macroscopic properties. This is a big step forward in predictive hierarchical materials modeling.

Acknowledgements

The authors gratefully acknowledge the financial support of the Deutsche Forschungsgemeinschaft (DFG) within the Collaborative Research Center (SFB) 761 “Steel–ab initio”. The authors would also like to give special thanks to Luc Hantcherli for his help with some of the figures.

References

[1] Allain S, Chateau JP, Bouaziz O. Mat Sci Eng A 2004;387:143.
[2] Barbier D, Favier V, Bolle B. Mat Sci Eng A 2012;540:212.
[3] Bouaziz O, Guelton N. Mat Sci Eng A 2001;319:246.
[4] Karaman I, Sehitoglu H, Beaudoin AJ, Chumlyakov YI, Maier HJ, Tome CN. Acta Mat 2000;48(9):2031.
[5] Shiekhelsouk MN, Favier V, Inal K, Cherkaoui M. Int J Plast 2009;25(1):105.
[6] Dancette S, Delannay L, Renard K, Melchior MA, Jacques PJ. Acta Mat 2012;60(5):2135.
[7] Gutierrez-Urrutia I, Zaefferer S, Raabe D. Scripta Mat 2009;61(7):737.
[8] Gutierrez-Urrutia I, Raabe D. Acta Mat 2011;59(16):6449.
[9] Gutierrez-Urrutia I, Raabe D. Acta Mat 2012;60:5791.
[10] Grabowski B, Hickel T, Neugebauer J. Phys Rev B 2007;76:024309.
[11] Friak M, Hickel T, Körmann F, Udyansky FA, Dick A, von Pezold J, et al. Steel Res 2011;82:86.
[12] Reeh S, Music, Gebhardt DT, Kasprzak M, Jäpel T, Zaefferer S, et al. Acta Mat 2012;60(17):6025–32.
[13] Saeed-Akbari A, Schwedt A, Bleck W. Scripta Mater 2012;66:1024.
[14] Ma A, Roters F. Acta Mat 2004;52(12):3603.
[15] Ma A, Roters F, Raabe D. Acta Mat 2006;54(8):2169.
[16] Adler P, Olson G, Owen W. Met Mat Trans A 1986;17(10):1725.
[17] Asgari S, ElDanaf E, Kalidindi SR, Doherty RD. Met Mat Trans A 1997;28(9):1781.
[18] El-Danaf E, Kalidindi SR, Doherty RD. Int J Plast 2001;17(9):1245.
[19] Hutchinson B, Ridley N. Scripta Mat 2006;55(4):299.
[20] Jin JE, Lee YK. Mat Sci Eng A 2009;527(1-2):157.
[21] Kalidindi SR. Int J Plast 2001;17(6):837.
[22] Kocks UF. Phil Mag 1966;13(123):541.
[23] Nes E. Prog Mat Sci 1997;41(3):129.
[24] Sevillano JG. Scripta Mat 2009;60(5):336.
[25] Rémy L. Met Trans A 1981;12(3):387.
[26] Venables JA. Deformation twinning. New York: Gordon & Breach; 1964.
[27] Friedel J. Dislocations. Oxford: Pergamon Press; 1965.
[28] Mahajan S. Phil Mag 1971;23(184):781.
[29] Mahajan S, Chin GY. Acta Metal 1973;21(10):1353.
[30] Gutierrez-Urrutia I, Zaefferer S, Raabe D. Mat Sci Eng A 2010;527(15):3552.
[31] Gutierrez-Urrutia I, Raabe D. Scripta Mat 2012;66:992.
[32] Rémy L. Acta Metal 1978;26:443.
[33] Christian JW, Mahajan S. Prog Mat Sci 1995;39(1–2):1.
[34] Kalidindi SR. J Mech Phys Sol 1998;46(2):267.
[35] Kalidindi SR. Int J Plast 1998;14(12):1265.
[36] Jia N, Roters F, Eisenlohr P, Kords C, Raabe D. Acta Mat 2012;60:1099.
[37] Jia N, Eisenlohr Pand Roters F, Raabe D. Acta Mat 2012;60:3415.
[38] Tomé CN, Lebensohn RA, Kocks UF. Acta Metal Mat 1991;39(11):2667.
[39] Allain S, Chateau JP, Bouaziz O. Steel Res 2002;73(6-7):299.
[40] Cherkaoui M. Phil Mag 2003;83(31–34):3945.
[41] Bouaziz O, Allain S, Scott C. Scripta Mat 2008;58(6):484.
[42] Mingxin H, Bouaziz O, Barbier D, Allain S. J Mat Sci 2011;46(23):7410.
[43] Rémy L. Acta Metal 1977;25(2):173.
[44] Mahajan S, Barry DE, Eyre BL. Phil Mag 1970;21(169):43.
[45] Kim J, Estrin Y, Beladi H, Timokhina I, Chin KG, Kim SK, et al. Met Mat Trans A 2012;43A(2):479.
[46] Cottrell AH, Bilby BA. Phil Mag 1951;42(329):573.
[47] Venables JA. Phil Mag 1961;6(63):379.
[48] Blewitt TH, Coltman RR, Redman JK. J Appl Phys 1957;28(6):651.
[49] Seeger A. Z Metallkunde 1956;47(9):653.
[50] Cohen JB, Weertman J. Acta Metal 1963;11(8):996.
[51] Cohen JB, Weertman J. Acta Metal 1963;11(8):1368.
[52] Fujita H, Mori T. Scripta Metal 1975;9(6):631.
[53] Miura S, Takamura JI, Narita N. Trans Jpn Inst Metals 1968;S 9:555.
[54] Kibey S, Liu JB, Johnson DD, Sehitoglu H. Acta Mat 2007;55(20):6843.
[55] Kibey SA, Wang LL, Liu JB, Johnson HT, Sehitoglu H, Johnson DD. Phys Rev B 2009;79(21):214202.
[56] Bracke L, Kestens L, Penning J. Scripta Mat 2009;61(2):220.
[57] Idrissi H, Renard K, Ryelandt L, Schryvers D, Jacques PJ. Acta Mat 2010;58(7):2464.
[58] Wietbrock B, Xiong W, Bambach M, Hirt G. Steel Res Int 2011;82(1):63.
[59] Wilkinson AJ, Anstis GR, Czernuszka JT, Long NJ, Hirsch PB. Phil Mag A 1993;68(1):59.

[60] Wilkinson AJ, Hirsch PB. Micron 1997;28(4):279.
[61] Gutierrez-Urrutia I, Raabe D. Scripta Mat 2012;66(6):343.
[62] Barbier D, Gey N, Allain S, Bozzolo N, Humbert M. Mat Sci Eng A 2009;500(1–2):196.
[63] Renard K, Jacques PJ. Mat Sci Eng A 2012;542:8.
[64] Roters F, Raabe D, Gottstein G. Acta Mat 2000;48(17):4181.
[65] Mecking H, Kocks UF. Acta Metal 1981;29(11):1865.
[66] Kocks UF, Argon AS, Ashby MF. Prog Mat Sci 1975;19:1.
[67] Estrin Y, Mecking H. Acta Metal 1984;32(1):57.
[68] Fullman RL. Trans AIME. 1953.
[69] Saeed-Akbari A, Mosecker L, Schwedt A, Bleck W. Metall Mater Trans A 2012;43:1688.
[70] Gottstein G. Physical Foundations of Materials Science. Berlin, Heidelberg: Springer; 2004.
[71] Chen L, Kim HS, Kim SK, De Cooman BC. ISIJ Int 2007;47(12):1804.
[72] Xiong ZP, Ren XP, Bao WP, Li SX, Qu HT. Mat Sci Eng A 2011;530(0):426.
[73] Eisenlohr A, Gutierrez-Urrutia I, Raabe D. Acta Mat 2012;60:3994.
[74] Zhao Z, Roters F, Mao W, Raabe D. Adv Eng Mater 2001;3:984.
[75] Raabe D, Klose P, Engl B. Adv Engin Mater 2002;4:169.
[76] Roters F, Eisenlohr P, Hantcherli L, Tjahjanto DD, Bieler TR, Raabe D. Acta Mat 2010;58(4):1152.
[77] Misra RDK, Zhang Z, Venkatasurya PKC, Somani MC, Karjalainen LP. Mat Sci Eng A 2011;528(3):1889.
[78] Herrera C, Ponge D, Raabe D. Acta Mat 2011;59:4653.
[79] Karaman I, Sehitoglu H, Gall K, Chumlyakov YI, Maier HJ. Acta Mat 2000;48(6):1345.
[80] Thornton PR, Mitchell TE. Phil Mag 1962;7(75):361.
[81] Suzuki H, Barrett CS. Acta Metal 1958;6(3):156.
[82] Dastur YN, Leslie WC. Met Trans A 1981;12(5):749.
[83] Owen WS, Grujicic M. Acta Mat 1998;47(1):111.